

A Model for Tunneling-Limited Breakdown in High-Power HEMTs

Mark H. Somerville and Jesús A. del Alamo

Massachusetts Institute of Technology, Cambridge, MA, U.S.A.

Abstract

We present a new predictive model for off-state breakdown in InAlAs/InGaAs and AlGaAs/InGaAs power high electron mobility transistors (HEMTs). The proposed model suggests that electron tunneling from the gate edge, and not impact ionization, is responsible for off-state breakdown in these devices. The model indicates that the crucial variables in determining the off-state breakdown voltage of power HEMTs are the sheet carrier concentration in the extrinsic gate-drain region, and the gate Schottky barrier height. Other design parameters have only secondary impact on the breakdown voltage for realistic device designs.

Introduction

Although initially targeted at low-noise applications, InAlAs/InGaAs and AlGaAs/InGaAs high electron mobility transistors (HEMTs) are enjoying significant success in microwave and millimeter wave power applications [1-4]. This has been accompanied by major strides towards the improvement of off-state breakdown in these devices through the use of novel recess, cap, channel, and insulator designs [5-8].

As impressive as recent reports of breakdown voltage improvement are, work in this area has been largely empirical, and has relied primarily on know-how gained from models of MESFET breakdown [9-11]. MESFET models are based upon the assumption that impact ionization determines the off-state breakdown voltage. The portability of these models should be questionable just on the grounds that modern power HEMT geometries differ substantially from MESFETs.

Recently several authors have suggested that impact ionization alone cannot explain the off-state breakdown behavior of HEMTs. Bahl et al. have proposed a two-step mechanism in which electrons injected from the gate initiate impact ionization in the channel [12]; Crosnier et al. appeal to tunneling in off-state as well [13]. Nonetheless, no *predictive* model currently exists for the off-state breakdown voltage of HEMTs. This hampers first-pass design success. Motivated by mounting experimental evidence that off-state breakdown is largely determined by tunneling and/or thermionic field emission [12, 14], and not simply impact ionization, we propose a new model for tunneling-limited breakdown in power HEMTs.

Experimental Background

In Fig. 1 we plot the results of several temperature-dependent studies of HEMT breakdown voltage (BV) in the AlGaAs/InGaAs system and the InAlAs/InGaAs system. Also plotted are recently reported results for a modern GaAs MESFET design. Strikingly, *all* these devices

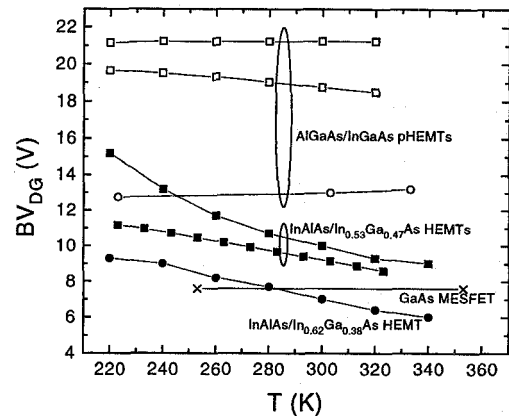


Figure 1: Temperature dependence of BV_{DG} in a variety of HEMT and MESFET structures. BV_{DG} almost uniformly exhibits temperature dependence close to or less than zero. This implies that tunneling and thermionic field emission are the dominant breakdown mechanisms. Data taken from [12, 14-16]

exhibit BV with temperature coefficients close to or less than zero. Of course, were impact ionization the dominant mechanism, we would expect a positive temperature coefficient, for although there is some discussion of the temperature dependence of impact ionization in InGaAs on InP, the suppression of impact ionization with increasing temperature in the GaAs system is well-known [8].

These results suggest that while impact ionization may play some role in the BV mechanism, BV is dominated by tunneling or thermally-assisted tunneling. Gate-current reverse-bias barrier height extractions offer confirmation that a thermally assisted tunneling mechanism is responsible for off-state breakdown. Both in the AlGaAs/InGaAs system and in the InAlAs/InGaAs system, such extractions yield low activation energies (< 0.2 eV) which drop as V_{DG} increases [12, 14].

Model

To understand how tunneling can limit BV, we first examine the geometry of a typical power HEMT (Fig. 2). If indeed tunneling is the dominant mechanism, determination of BV boils down to an electrostatics problem: for a given V_{DG} , what is the magnitude of the field beneath the drain end of the gate? Once this field and the Schottky barrier height (ϕ_B) are known, determination of tunneling (or thermionic field emission) current is straight-forward.

In typical power HEMT designs, two physical observations allow us to construct a simple model for the electrostatics. First, as V_{DG} is increased, a depletion region of

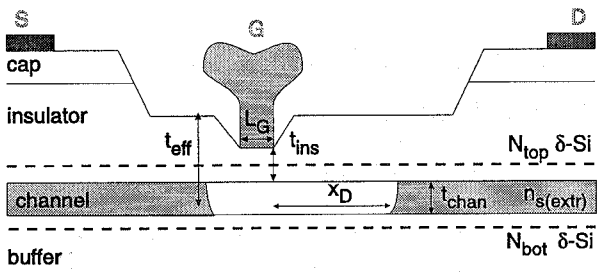


Figure 2: Cross-section of a typical power HEMT. x_D is defined as the length of the drain depletion region measured from the drain edge of the gate; $n_{s(extr)}$ is the sheet carrier concentration in the extrinsic (wide recess) region; and N_{top} and N_{bot} are respectively the top and bottom doping levels.

length x_D opens up in the extrinsic portion of the channel starting from the drain side of the gate; all the depleted charge from this region must be imaged on the gate. Second, in well-designed power HEMTs x_D is significantly greater than the vertical dimensions t_{chan} and t_{ins} . When x_D is large, the geometry of this problem becomes virtually one-dimensional, so that the field on the drain end of the gate will not depend much on insulator thickness, channel thickness, doping ratio, or gate length. Indeed, the only relevant parameters to determine the field in this picture are x_D and the extrinsic sheet carrier concentration ($n_{s(extr)}$). If $n_{s(extr)}$ is constant over x_D , the field beneath the gate is proportional to x_D .

With these physical insights in mind, we propose the simplified field distribution outlined in Fig. 3: for $V_{DG} = V_T$, the field beneath the gate is constant at E_T ; as V_{DG} grows, all additional depletion charge is imaged across the gate according to some distribution that is independent of x_D , so that at any point on the gate the total additional field is proportional to both x_D and $n_{s(extr)}$. We further expect the field beneath the gate to be strongly peaked at the drain end of the gate, reaching a value $E_{gate(max)}$. Finally, in the depleted portion of the drain, the field should have a triangular shape, as the depletion approximation demands. Thus, $E_{gate(max)}$ should rise as the square root of V_{DG} .

The simplifications we propose are borne out by examination of Frenslley's MESFET avalanche breakdown model, which solves the field distribution in a simplified (semi-infinite gate) case [11]. The model predicts that when the depletion length is greater than the vertical dimension of the problem, differential changes in x_D produce a differential increase in field at the gate edge that is independent of x_D and only weakly dependent on the insulator thickness. Indeed, when $x_D \geq t_{eff}$, we can write the field beneath the gate as

$$E_{gate}(x) \approx \frac{qn_{s(extr)}x_D}{\epsilon_s} \frac{2}{\pi(1 + \frac{4x}{\pi t_{eff}})\sqrt{\pi t_{eff}x}} + E_T \quad (1)$$

where t_{eff} is the location of the centroid of charge (nominally the distance from the surface to the center of the channel), and E_T is the field beneath the gate at threshold. Calculation of V_{DG} in the $x_D \geq t_{eff}$ case becomes

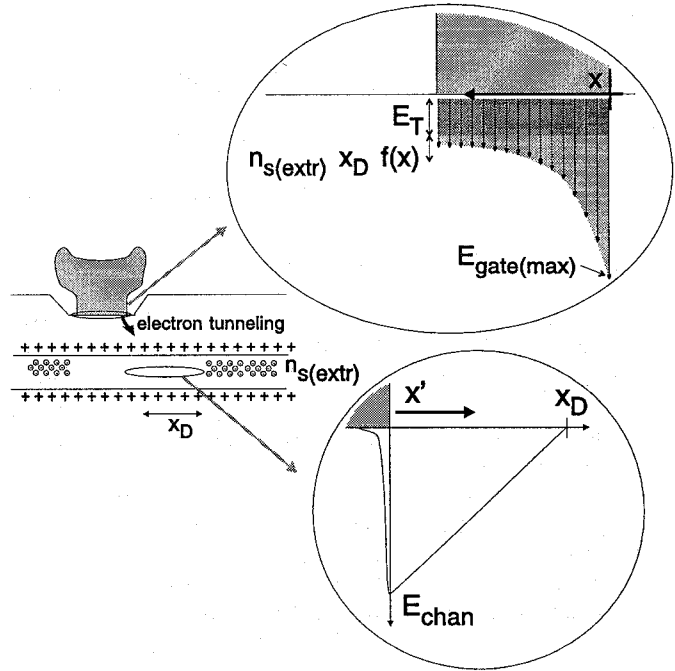


Figure 3: Illustration of postulated field profile beneath the gate, E_{gate} , and in the extrinsic drain, E_{chan} . E_{gate} is strongly peaked at the drain end of the gate, and obeys a simple functional description that depends only on the carrier concentration in the extrinsic region and the extent of lateral depletion. E_{chan} has a triangular shape given by a depletion approximation. We define the coordinate x as the lateral position beneath the gate measured from the gate edge, while the coordinate x' is the lateral distance within the channel measured from the gate edge towards the drain.

relatively simple as well; to first order,

$$V_{DG} - V_T \approx \frac{0.7qn_{s(extr)}x_D^2}{2\epsilon_s t_{eff}} \quad (2)$$

Eq. (2) is then substituted into (1) to determine the field-voltage relationship:

$$E_{gate}(x) - E_T \approx \sqrt{\frac{2.8qn_{s(extr)}(V_{DG} - V_T)}{\epsilon_s} \frac{2}{\pi(1 + \frac{4x}{\pi t_{eff}})\sqrt{\pi x}}} \quad (3)$$

Note that as is the case in avalanche models [9, 11], the field near the gate edge (which determines the tunneling current) has virtually no dependence on t_{eff} .

Of course, such a model is not entirely appropriate for calculating tunneling current, given that the field diverges at the gate edge. This effect arises from the fact that the transformation does not consider the gate corner accurately. To account for this we cut off the field at some finite distance ($\sim 70 \text{ \AA}$) from the gate corner [17]. Gate current is then calculated easily:

$$I_G = \int_{x_{min}}^{L_G} \frac{q^2 m_0 E_{gate}^2(x)}{8\pi h m^* \phi_B} \exp\left[\frac{-4\sqrt{2qm^*}\phi_B^{3/2}}{3\hbar E_{gate}(x)}\right] dx \quad (4)$$

BV is defined as the value of V_{DG} that gives rise to a certain value of I_G , typically 1 mA/mm.

2.3.2

Parameter	Simulated Values	Units
t_{ins}	180, 220, 270	Å
t_{chan}	130, 220, 300	Å
L_G	0.1, 0.25, 0.5	μm
N_{tot}	3, 4, 5	10^{12}cm^{-2}
N_{top}/N_{bot}	3/2, 4/1, 5/0	-
ΔE_C	0.3, 0.5	eV

Table 1: Values of varied device parameters in 2D simulations. Note that all device parameters are centered about realistic values for state-of-the-art devices.

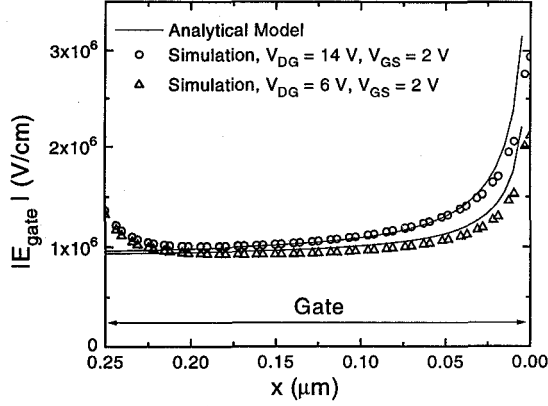


Figure 4: Comparison of simulated and calculated field profiles beneath the gate for two bias conditions. The model accurately captures the strong peak in electric field at the drain end of the gate.

Discussion

In order to validate this model, we have performed extensive electrostatic simulations of realistic HEMT structures (Fig. 2) using MEDICI. The values of variable parameters are listed in Table 1. From these simulations, we have extracted the magnitude of the field beneath the gate for two bias conditions (Fig. 4). Also plotted are the field distributions predicted by the model.

As can be seen, the simplistic model we have proposed describes the shape of the field extremely well everywhere but at the source end of the gate, where the semi-infinite gate assumption becomes invalid. Simulations also show that our triangular description of the field in the channel is appropriate except in the immediate vicinity of the gate edge, where $x' \approx t_{eff}$ (Fig. 5). The model accurately predicts the length of the depletion region under realistic bias conditions for a variety of $n_{s(extr)}$ values (Fig. 6); as can be seen, $E_{gate(max)}$ depends linearly on x_D . Most importantly, the model yields the voltage-field relationship that is necessary to calculate the tunneling current (Fig. 7).

Examination of the leading terms in (2) and (3) makes it clear that the crucial parameter in determining breakdown due to tunneling is the carrier concentration in the extrinsic region. In order to explore this issue from a design perspective, we have performed a simple sensitivity analysis for the field beneath the gate at a given bias condition. A state-of-the-art device design was chosen

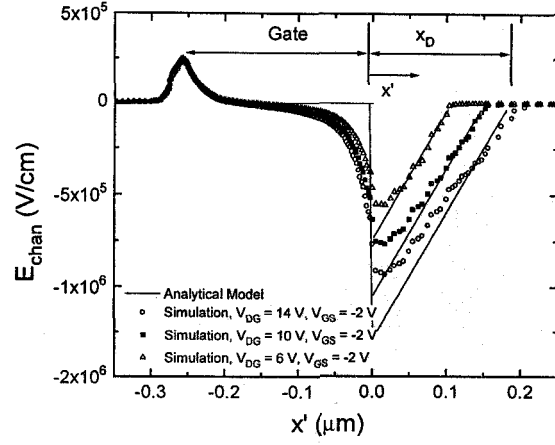


Figure 5: Simulated and calculated lateral field profile within the channel. For all values of V_{DG} the field displays a triangular behavior as demanded by the depletion approximation.

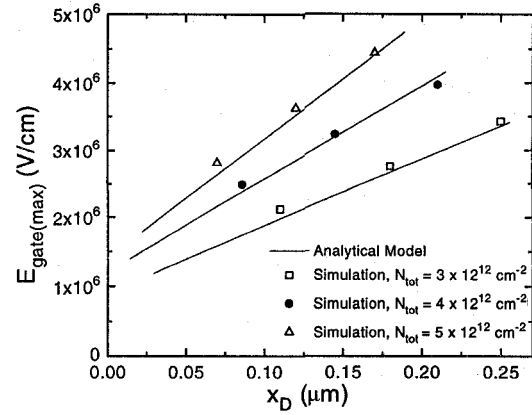


Figure 6: Simulated and calculated dependence of the maximum field at the drain end of the gate, $E_{gate(max)}$, on the length of the depletion region, x_D . The linear behavior indicates that the depletion charge is being imaged in accordance with the simple picture we propose ($x_{min} = 70$ Å).

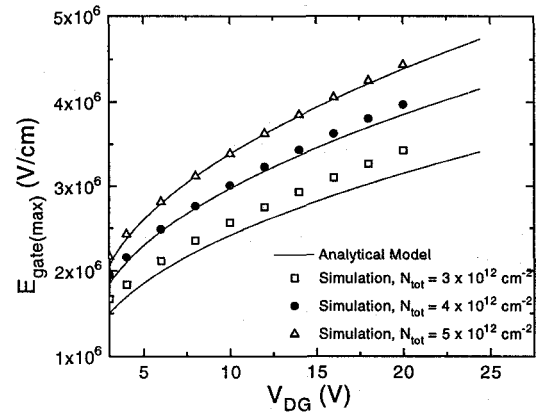


Figure 7: V_{DG} vs. $E_{gate(max)}$ from analytic model and 2D simulations ($x_{min} = 70$ Å).

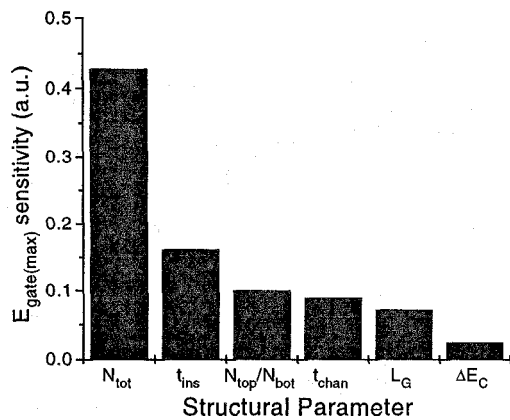


Figure 8: Sensitivity of maximum field beneath the gate to different structural parameters. N_{tot} , which establishes the sheet carrier concentration in the extrinsic region, emerges as the most critical structural parameter.

as a baseline, and each design parameter of interest was individually varied to assess its impact on E_{gate} . All parameters were only varied within realistic boundaries for modern devices (values given in Table 1). Our simulations clearly confirm the physical insight that for realistic designs, $E_{gate(max)}$ and the distribution of the field beneath the gate should depend strongly on $n_s(extr)$, and should be independent of most other variables. Indeed, modifications to t_{chan} , t_{ins} , L_G , doping ratio N_{top}/N_{bot} , and ΔE_C between insulator and channel had relatively little impact on E_{gate} so long as the total doping level (N_{tot}) was held constant and the recess length on the drain was sufficient to accommodate x_D (Fig. 8). Our analysis establishes N_{tot} , which sets $n_s(extr)$, as the single most important parameter in determining E_{gate} .

Using our model, we can predict the tunneling current and the resulting BV limit in power HEMTs. Fig. 9 plots the tunneling-limited BV as a function of $n_s(extr)$ and ϕ_B (for $I_G = 1$ mA/mm). Also included in the figure are the results of several relatively well-controlled experiments varying $n_s(extr)$ in both the InAlAs/InGaAs system and in the AlGaAs/InGaAs system; as can be seen, the data behaves as the model predicts. Furthermore, the experiments indicate that the potential for improving BV without modifying $n_s(extr)$ or ϕ_B appears to be limited.

Note that Fig. 9 includes both lattice-matched and strained channel data for the InAlAs/InGaAs system. The similarity between the strained and lattice-matched data is striking. This suggests the lower BV typically observed in high-indium channels is not due to enhanced impact ionization, but rather results from the increased $n_s(extr)$ usually achieved in such designs.

Conclusions

In summary, we have proposed a simple physical model for tunneling-limited off-state BV in HEMTs. Two critical parameters limit BV in power HEMTs: $n_s(extr)$ and ϕ_B . Our model can also easily be extended to incorporate the additional reduction in BV arising from thermionic field emission.

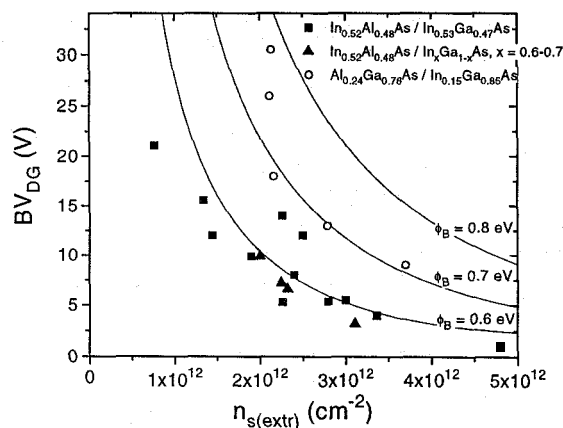


Figure 9: Predicted tunneling-limited breakdown voltage ($I_G = 1$ mA/mm) as a function of extrinsic carrier concentration and barrier height. For non-selective recess technologies, $n_s(extr)$ is calculated based on I_{Dmax} . Note that InGaAs/InAlAs data obeys the expected trend regardless of indium content in the channel. The graph establishes the maximum attainable breakdown voltage for a given gate technology and extrinsic carrier concentration. Data from [1, 6, 12, 18, 19].

Acknowledgments

This work was partially supported by Lockheed-Martin and JSEP (DAAH04-95-1-0038).

References

1. J. J. Brown et al., *IEEE Micro. Guided Wave Lett.*, **6**, 91 (1996).
2. M. Aust et al., *IEEE Micro. Guided Wave Lett.*, **5**, 12 (1995).
3. S. W. Chen et al. *IEEE Micro. Guided Wave Lett.*, **5**, 201 (1995).
4. P. M. Smith et al., *IEEE Micro. Guided Wave Lett.*, **5**, 230 (1995).
5. J. C. Huang et al., *IEEE Trans. Micro. Theory Tech.*, **41**, 752 (1993).
6. K. Y. Hur et al., *IEEE GaAs IC Symp.*, 101 (1995).
7. S. R. Bahl and J. A. del Alamo, *IEEE Elect. Dev. Lett.*, **13**, 123 (1992).
8. G. Meneghesso et al., *54th Dev. Res. Conf.*, 138 (1996).
9. S. H. Wemple et al. *IEEE Trans. Elect. Dev.*, **ED-27**, 1013 (1980).
10. C. Chang and D. S. Day, *Solid-State Elect.*, **32**, 971 (1989).
11. W. Frensley, *IEEE Trans. Elect. Dev.*, **ED-28**, 962 (1981).
12. S. R. Bahl et al., *IEEE Trans. Elect. Dev.*, **42**, 15 (1995).
13. Y. Crosnier, *24th Eur. Micro. Conf.*, **1**, 88 (1994).
14. M. Somerville et al., *54th Dev. Res. Conf.*, 140 (1996).
15. C. Tedesco et al., *IEEE Trans. Elect. Dev.*, **40** 1211 (1993).
16. C. Gaquiere et al., *IEEE Trans. Elect. Dev.*, **42** 209 (1995).
17. H. Muto et al., *1993 Intl. Conf. Sol. Stat. Dev. and Mats.*, 264 (1993).
18. S. R. Bahl, Ph.D. dissertation, M.I.T. (1993)
19. H. Rohdin et al. *7th Intl. Conf. on InP and Rel. Mat.*, 73 (1995).